Identification of sea ice at low incidence angles using Ku-band radar data onboard GPM satellite

Maria Panfilova [(1)]
(1) Institute of applied physics RAS, Nizhny Novgorod, Russia

Abstract

The method for identification of sea ice from the data of Ku-band radar onboard GlobalPrecipitation Measurement (GPM) satellite is outlined. It was shown before that the dependence of normalized radar cross section on incidence angle differs for clear sea and ice covered surface. The kurtosis of surface slopes probability density function was calculated. Sea ice concentration was obtained from radiometer GPM microwave imager (GMI) data onboard GPM satellite. The threshold for kurtosis was chosen basing on sea ice concentration data.

1 Introduction

Sea ice identification using microwave instruments is an important problem, especially in Arctic and Antarctic regions. Dual frequency precipitation radar (DPR) onboard GPM satellite observes the globe within ±65° latitude, thus polar areas where ice presents are partially covered.

In previous work the method for automatic ice detection using Ku-band DPR data was developed [1]. In the present work the method is validated using GMI and AMSR radiometers data in Arctic and Antarctic regions.

2 Data

The GPM satellite was launched in February 2014, carrying five instruments including the DPR and radiometer GPM Microwave Imager (GMI). The satellite ground track is confined between 65° S and 65° N. The DPR is a Ku- and Ka-band pulsed radar with horizontal polarization, further we consider Ku-band radar only because it had a wider ground track in 2016. The DPR antenna scans perpendicularly to the flight direction. The scanning angle varies from -17° to +17°, with 49 beam positions separated by 0.71°. The local incidence angle depends on the shape of the Earth. Maximum local incidence angle is approximately 18°, spatial resolution is about 5 km by 5 km. The GPM data contains a rain flag for each resolution element.

GMI is a conically scanning multychannel microwave radiometer. It is also installed onboard GPM satellite. Its swath is 885 km. Sea ice concentration (SIC) was calculated from GMI data using the algorithm [2] and collocated with DPR measurements.

The data for January 2018 was used for Northern hemisphere and the data for July 2018 was used for Southern hemisphere. In figure 1 the example of the dependence of normalised radar cross section (NRCS) over water and ice surface is presented.

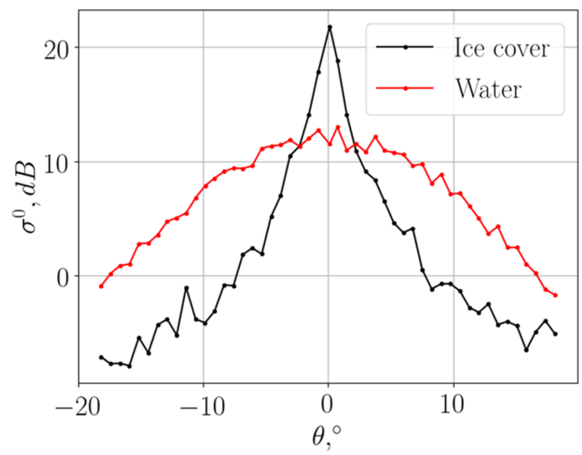

Figure 1. The example of the dependence of normalised radar cross section (NRCS) over water and ice surface (from [1])

In figure 2 the PDF of NRCS over ice and water surface is presented for incidence angle 1.5°. It can be clearly seen that sea ice detection basing on NRCS is difficult. Thus the approach based on the knowledge of statistics of surface slopes was adopted.

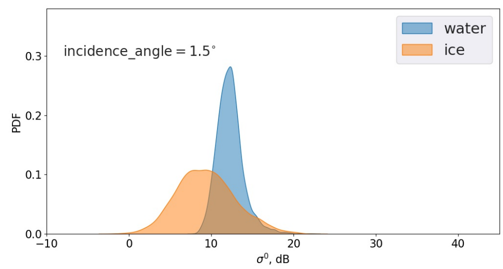

Figure 2. PDF of NRCS over ice and water surface for incidence angle 1.5°.

3 Sea ice detection method

Let us briefly remind the idea from [1] of sea ice detection using the information on surface statistics.

According to geometrical optics (GO) approximation NRCS is proportional to the slope probability density function (PDF) along the direction of scanning [3]

$$\sigma^0 = A\cos^{-4}(\theta)\cdot P(\tan\theta) \qquad (1)$$

PDF of water surface slopes is close to Gaussian, while the sea ice the has the narrow peak at $\theta = 0°$. The sharper is the curve peak near the center of distribution, the greater is the value of the kurtosis coefficient of PDF. The kurtosis coefficient for $P(x)$ is calculated as follows

$$\gamma_2 = \frac{\mu_4}{\mu_2^2} - 3, \qquad (2)$$

where μ_2 and μ_4 are the central statistical moments of PDF

$$\mu_k = \int_{-\infty}^{\infty} (x-\bar{x})^k P(x)dx \qquad (3)$$

and $\bar{x}$ is the expected value of x:

$$\bar{x} = \int_{-\infty}^{\infty} xP(x)dx. \qquad (4)$$

For DPR data if we consider the part of the scan for $-15° < \theta < 15°$ (where GO approximation is valid), $N = 41$, μ_k in a discrete form is as follows

$$\mu_k = \sum_{i=1}^{N}(\tan\theta_i - \overline{\tan\theta_i})^k \sigma_i^0 \cos^4(\theta_i)\left[\sum_{i=1}^{N}\sigma_i^0\cos^4(\theta_i)\right]^{-1}. \qquad (5)$$

Each half of the swath can be considered separately for $\theta > 0°$ and $\theta < 0°$. In order to calculate kurtosis properly each half is complemented symmetrically so that $\sigma^0(\theta) = \sigma^0(-\theta)$ and for each augmented half-scan the operations (2)-(5) are performed.

The threshold of kurtosis for sea ice discrimination from water was obtained as follows. Basing on GMI data the footprints with $SIC < 0.1$ were marked as water, and with $SIC \geq 0.1$ were marked as ice.

Basing on DPR data the footprint was labeled as ice if $\gamma_2 > \tilde{\gamma}_2$ for the half-scan where the footprint belongs. In order to obtain optimal threshold value $\tilde{\gamma}_2$, F-score was maximized. F-score is calculated as follows

$$F = \frac{TP}{TP + 0.5(FP + FN)}, \qquad (6)$$

where TP (true positive) is the quantity of footprints where $SIC \geq 0.1$ and $\gamma_2 \geq \tilde{\gamma}_2$, FP (false positive) is the quantity of footprints where $SIC < 0.1$ and $\gamma_2 \geq \tilde{\gamma}_2$, and FN (false negative) is the quantity of footprints where $SIC \geq 0.1$ and $\gamma_2 < \tilde{\gamma}_2$.

Optimization was performed for the central part of the swath ($|\theta| < 4.5°$), for $F = 0.95$ the threshold value $\tilde{\gamma}_2 = 3$.

4 Results

The data for the first decade of January and first decade of July were processed for Northern and Southern hemispheres respectively. Sea ice is marked with blue. The position of sea ice from DPR data is shown in figures 3 and 4, and sea ice concentration from AMSR data (University of Bremen archive) is shown in figures 5 and 6. Good agreement is observed.

5 Conclusions

New method for sea ice detection using DPR data was validated using radiometer data. The idea of the method is to use the information on statistical properties of underlying surface. The advantage of the approach is that exact calibration of the instrument is not important.

6 Acknowledgements

This work is supported by RSF grant 20-17-00179.

References

[1] M. Panfilova, A. Shikov and V. Karaev, "Sea ice detection using Ku-band radar onboard GPM satellite," *2020 XXXIIIrd General Assembly and Scientific Symposium of the International Union of Radio Science*, 2020, pp. 1–3, doi: 10.23919/URSI-GASS49373.2020.9232361.

[2] G. Spreen, L. Kaleschke, G. Heygster, "Sea ice remote sensing using AMSR-E 89–GHz channels," *J.Geophys. Res. Oceans*,**113**, C2, 2008, pp. 1978—2012, doi: 10.1029/2005JC003384.

[3] F. G. Bass and I. M. Fuks, "Scattering of waves by statistically rough surfaces," Pergamon Press, 1972.

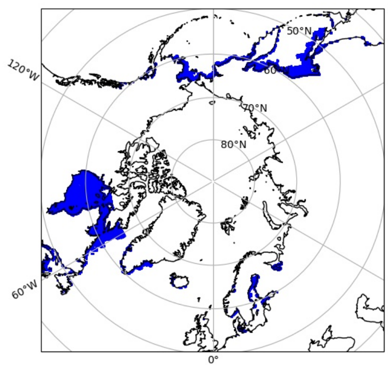

Figure 3. Sea ice from Ku-band DPR data in Northern hemisphere, first decade of January.

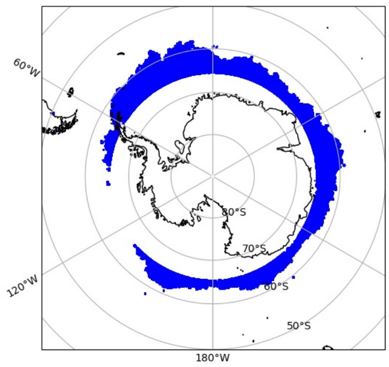

Figure 4. Sea ice from Ku-band DPR data in Southern hemisphere, first decade of July

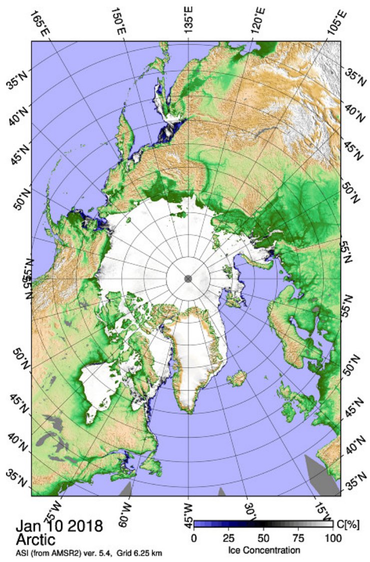

Figure 5. Sea ice from AMSR data in Northern hemisphere, January 10.

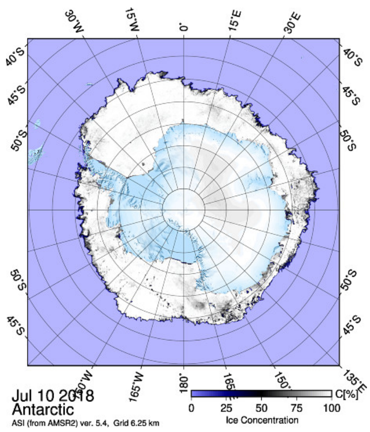

Figure 6. Sea ice from AMSR data in Southern hemisphere, July 10.